

Multiplicity of vortex soliton families in the discrete Ginzburg-Landau equation, their interactions and the formation of bound states

C. Mejía-Cortés and J.M. Soto-Crespo

Instituto de Óptica, C.S.I.C., Serrano 121, 28006 Madrid, Spain

Rodrigo A. Vicencio and Mario I. Molina

Departamento de Física, Facultad de Ciencias, Universidad de Chile, Casilla 653, Santiago, Chile and

Center for Optics and Photonics (CEFOP), Casilla 4016, Concepción, Chile

(Dated: November 7, 2011)

By using different continuation methods, we unveil a wide region in the parameter space of the discrete cubic-quintic complex Ginzburg-Landau equation, where several families of stable vortex solitons coexist. All these stationary solutions have a symmetric amplitude profile and two different topological charges. We also discover the dynamical formation of a variety of ‘bound-state’ solutions, composed of two or more of these vortex solitons. All of these stable composite structures persist in the conservative cubic limit, for high values of their power content.

I. INTRODUCTION

Optical beams whose phase circulates around a singular point -or central core-, changing by $2\pi S$ times in each closed loop around it (with S being an integer number), are called optical vortices. The integer number S is known as the topological charge of the vortex, and its sign defines the direction of the phase circulation. Usually an optical vortex has a doughnut-like shape and diffracts when it propagates in free space. In quantum information they have an enormous potential for codifying information beyond two levels using their topological charge value [1]. In other fields, such as biophotonics for example, they are useful due to their ability to affect the motion of particles (microorganisms) through angular momentum transfer [2]. Other scientific and technological applications for optical vortices are found in optical systems communication, spintronics and optical tweezers [3–5]. These potential applications of optical vortices have sparked the interest of the scientific community on their basic properties and characteristics.

Diffraction is a fundamental phenomenon which leads to beam broadening upon propagation. In a nonlinear medium, self-focusing reduces diffraction whereas self-defocusing enhances the beam spreading. In a situation where the nonlinear self-focusing effects exactly balances diffraction, the beam can propagate as an optical spatial soliton, i.e. a self-trapped optical beam which preserves its shape upon propagation. Recently, spatial optical solitons have become attractive for several technological applications. They can be defined as self-localized solutions of nonlinear wave equations found in various physical systems [6]. Typical equations of this type in optics are the nonlinear Schrödinger equation (NLSE) for conservative systems, and the complex Ginzburg-Landau equation (CGLE) for dissipative ones [7, 8]. The CGLE is a master model in which dissipative solitons [9] are probably its most interesting solutions. In conservative models, such as the ones described by the NLSE or its several variants, exchange of energy with the sur-

roundings is not allowed. Self-localized solutions for the nonlinear Schrödinger equation originate from a balance between nonlinearity (e.g., the Kerr effect) and dispersion/diffraction. In contrast, for dissipative systems the solutions also exchange energy with an external source, making the problem more complex and rich. In this case, an extra balance between gain and loss is required in order to obtain stationary solutions. In particular, dissipative vortex solitons in continuous media have been found to exist for several values of S , and they are stable in wide regions of the parameter space of the CGLE [20, 21].

In this paper we concentrate on dissipative systems governed by the Ginzburg-Landau equation. This model appears in many branches of science such as nonlinear optics, Bose-Einstein condensates, chemical reactions, super-conductivity and many others [10, 11]. Nonlinear periodic structures offer alternative ways to control light propagation by modifying its diffraction properties through the modulation of its refractive index. For instance, photonic crystals are structures of alternating refractive index that provide unprecedented control over light fields propagating through them; recent works show that lasers with square-lattices photonic crystal cavities possess enhanced functionality and performance when compared to conventional lasers [12]. These systems can be analyzed in the framework of a set of coupled, linear equations which, in solid-state physics is known as the *tight-binding* approximation, while in an optics context, it is known as the coupled-mode approach. Stationary solutions obtained in this framework are called discrete solitons. In particular, discrete vortex solitons in conservative systems have been reported on several theoretical and experimental works [16–19], while dissipative discrete solitons have been found, analytically and numerically, in one dimensional waveguide arrays [13–15].

In this paper we report the finding of a wide region in the parameter space of the discrete cubic-quintic complex Ginzburg-Landau equation where different discrete vortex solitons coexist. All the individual solutions we examine in this paper possess simultaneously two topo-

logical charges, as those reported in some of our recent works [22, 23]. We have studied their interactions and as a result the formation of bound states.

The rest of the paper is organized as follows. In Section II we introduce the complex cubic-quintic Ginzburg-Landau model that we will use in this work. Section III describes the new families of solutions we have found, and in Section IV we show the composite structures obtained when we let them interact as they evolve. Section V analyzes the discrete nonlinear Schrödinger equation case for all the solutions previously mentioned. Finally, section VI summarizes our main results and conclusions.

II. MODEL

Optical beam propagation in nonlinear, periodical two-dimensional waveguide array can be modeled by the following equation:

$$i\dot{\psi}_{m,n} + \hat{C}\psi_{m,n} + |\psi_{m,n}|^2\psi_{m,n} + \nu|\psi_{m,n}|^4\psi_{m,n} = i\delta\psi_{m,n} + i\varepsilon|\psi_{m,n}|^2\psi_{m,n} + i\mu|\psi_{m,n}|^4\psi_{m,n}. \quad (1)$$

Equation(1) is the discrete version of the complex cubic-quintic Ginzburg-Landau (CQGL) equation. Here, $\psi_{m,n}$ is the complex field amplitude at the (m, n) lattice site and $\dot{\psi}_{m,n}$ denotes its first derivative with respect to the propagation coordinate z . The set

$$\{m = -M, \dots, M\} \times \{n = -N, \dots, N\},$$

defines the array, with $2M + 1$ and $2N + 1$ being the number of sites in the horizontal and vertical directions, respectively. The *tight binding* approximation establishes that the field propagating in each waveguide interacts linearly only with nearest-neighbor fields through their evanescent tails. This interaction is described by the discrete diffraction operator

$$\hat{C}\psi_{m,n} = C(\psi_{m+1,n} + \psi_{m-1,n} + \psi_{m,n+1} + \psi_{m,n-1}),$$

where C is a complex parameter. Its real part denotes the strength of the coupling between adjacent sites and its imaginary part denotes the gain or loss originated by this coupling. The nonlinear higher-order Kerr term is represented by ν while $\varepsilon > 0$ and $\mu < 0$ are the coefficients for cubic gain and quintic losses, respectively. Linear losses are accounted by a negative value of δ .

In contrast to the conservative discrete nonlinear Schrödinger (DNLS) equation, the optical power, defined as

$$Q(z) = \sum_{m,n=-M,-N}^{M,N} |\psi_{m,n}(z)|^2, \quad (2)$$

is not a conserved quantity in the present model. Nevertheless, for a self-localized solution, the power and its evolution will be the main quantity that we will monitor in order to identify different families of stationary solutions.

We look for stationary solutions of Eq.(1) of the form $\psi_{m,n}(z) = \phi_{m,n} \exp(i\lambda z)$ where λ is real and $\phi_{m,n}$ are complex amplitudes. We are interested in solutions localized in space whose phase changes azimuthally by an integer number (S) of 2π along a discrete closed-circuit. In such a case, the self-localized solution is called a discrete vortex soliton [24] with vorticity S . By inserting the previous *ansatz* into Eq. (1) we obtain the following set of $(2M + 1) \times (2N + 1)$ algebraic coupled complex equations:

$$-\lambda\phi_{m,n} + \hat{C}\phi_{m,n} + |\phi_{m,n}|^2\phi_{m,n} + \nu|\phi_{m,n}|^4\phi_{m,n} = i\delta\phi_{m,n} + i\varepsilon|\phi_{m,n}|^2\phi_{m,n} + i\mu|\phi_{m,n}|^4\phi_{m,n}. \quad (3)$$

We solve Eq.(3) by using a multi-dimensional Newton-Raphson iterative algorithm. The method requires an initial guess, and it converges rapidly when using a highly-localized profile [more details can be found in Ref. [22]].

A. Linear stability analysis

Small perturbations around the stationary solution can grow exponentially, leading to the destruction of the vortex soliton. A stability analysis provides us with the means for establishing which solutions are linearly stable. Let us introduce a small perturbation $\tilde{\phi}$, to the localized stationary solution

$$\psi_{m,n} = [\phi_{m,n} + \tilde{\phi}_{m,n}(z)]e^{i\lambda z}, \quad \tilde{\phi}_{m,n} \in \mathbb{C}, \quad (4)$$

then, after replacing Eq.(4) into Eq.(1) and then linearizing with respect to $\tilde{\phi}$, we obtain:

$$\begin{aligned} &\dot{\tilde{\phi}}_{m,n} + \hat{C}\tilde{\phi}_{m,n} - i\delta\tilde{\phi}_{m,n} + \\ &[2(1 - \varepsilon)|\phi_{m,n}|^2 + 3(\nu - \mu)|\phi_{m,n}|^4 - \lambda]\tilde{\phi}_{m,n} + \\ &[(1 - \varepsilon)\phi_{m,n}^2 + 2(\nu - \mu)|\phi_{m,n}|^2\phi_{m,n}^*]\tilde{\phi}_{m,n}^* = 0. \end{aligned} \quad (5)$$

The solutions of the above homogeneous linear system can be written as

$$\tilde{\phi}_{m,n}(z) = C_{m,n}^1 \exp[\gamma_{m,n}z] + C_{m,n}^2 \exp[\gamma_{m,n}^*z], \quad (6)$$

where $C^{1,2}$ are integration constants and $\gamma_{m,n}$ is the discrete spectrum of the *eigensystem* associated with (5). The solutions are unstable if at least one eigenvalue has a positive real part, that is, if $\max\{\text{Re}(\gamma_{m,n})\} > 0$.

III. MULTIPLICITY OF STABLE VORTEX SOLITON FAMILIES

As stated above, the nonlinear gain in the system is mainly controlled by ε ; this parameter will be the only one that we will change in our simulations. Once we find a stationary solution - for a fixed set of parameters -, we compute its linear stability, and then change the parameters slightly and find the new solution using the previous

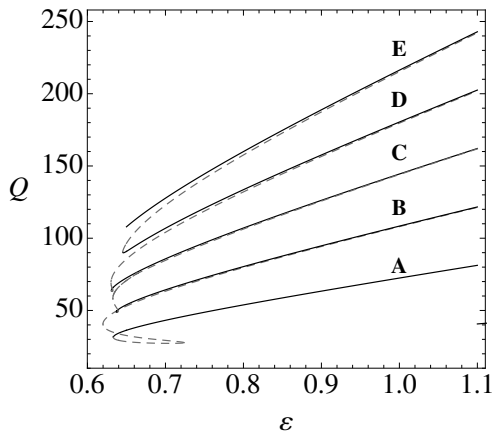


Figure 1. Q versus ε diagram for several vortex interconnected soliton families. Solid lines correspond to stable families while dashed lines to unstable ones. (CQGL equation parameters: $C = 0.8$, $\delta = -0.9$, $\mu = -0.1$, $\nu = 0.1$).

one as an *ansatz*. In this manner we obtain all the solution families displayed in the Q vs ε diagram shown in Fig.(1). The first of them (**A**-family), was already reported in our recent works [22, 23]. It was obtained by starting from the fundamental four-peaks discrete vortex soliton with $S = 1$, after passing throughout several saddle-node points. A striking property of all the solutions shown in Fig.(1) is that they have - simultaneously - two topological charges; i.e., they are two-charge vortices. Representative amplitude and phase profiles for these families are shown in Fig.(2).

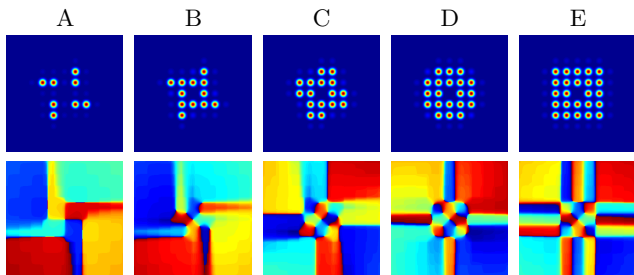


Figure 2. (Color online) Color map plots for the amplitude (top) and phase (bottom) profiles of stable vortex solutions for the families marked in Fig.(1).

Stable families **B**, **C**, **D** and **E** - shown in Figs.(1) and (2) - were unveiled after observing the dynamical evolution of solutions belonging to unstable branches (dashed gray lines). In some cases, the stable and unstable families are so close that they are nearly indistinguishable at the scale of Fig.(1). From the amplitude profiles we can see that there is a difference of four excited sites between one stable family and the next one. Family **A** has eight main excited sites and family **E** has twenty four main peaks. All these families show a coexistence of two topological charges.

The amplitude profile for case (**A**) shows a swirl spatial

configuration. From its phase profile we can identify a topological charge $S = 1$ in the core - the most inner discrete contour - and a charge $S = -3$ away from the center. The phase profiles for families **B**, **C**, **D** and **E** show a topological charge $S = -3$ in the core of these solutions. From **B** to **D**, the topological charge has the same value in the core and away from there, but the phase profile outside looks rotated respect to the center. For the last family, **E**, the topological charge has increased up to $S = -7$ away from the center.

IV. COMPOSITE STRUCTURES

Next, we study the formation of bound states composed of two vortex solitons belonging to the family **E** with $\varepsilon = 0.9$. We have chosen this family due to his high value of vorticity and squared symmetry equivalent to that of the optical lattice. We study dynamically the evolution of an array of two of these solutions, horizontally shifted by a certain small distance. We tested two initial configurations differing in their initial separation and, for each one of them we try a broad range of initial phase differences, following a procedure similar to the one implemented in Ref. [25]. For this purpose, we multiply the second solution by a phase factor $e^{i\theta_\alpha}$, where $\theta_\alpha \equiv \frac{\pi}{20}\alpha$ with $\alpha = 1, 2, \dots, 40$. A bound state is reached when the relative phase ($\Delta\theta$, defined as the phase difference between two given sites in each solution) becomes a constant. In continuous and homogeneous systems, the separation distance also changes along the evolution and it becomes a constant when the bound state is formed. Here, in the dissipative discrete case we do not observe any soliton mobility and, therefore, the separation distance remains invariant.

We have measured the phase difference, in both configurations, for the sites enclosed by the white circles showed in Fig.3(a). Figs.4(a) and (b) show $\Delta\theta$ and Q versus z , respectively, for the first configuration shown in Fig.3(a). We clearly identify two attraction basins, labeled as **b1** $^{\leftarrow}$ and **b1** $^{\rightarrow}$. Both (**b1** $^{\leftarrow}$) correspond to the lower power value shown in Fig.4(b). This implies that both basins are symmetrically equivalent solutions. The unstable configuration is labeled as **b2** and it corresponds to the upper power value in Fig.4(b) [Figs.3(c) and (d) show the amplitude and phase profiles of this unstable solution].

All these solutions preserve the central core structure, keeping the same topological charge as the initial input condition. Figs.3(a) and (c) show the amplitude profile for both of them; although they are very similar, the first one has an extra central core (marked by a red circle), located at the center of the structure. For the second structure we can note that the column in the middle ($m = 0$) is filled by small tails, without a central core. By taking a closed look at the rectangular contour sketched in Fig.3(b), we find that the phase varies continuously. The charge increases in the direction indicated by the

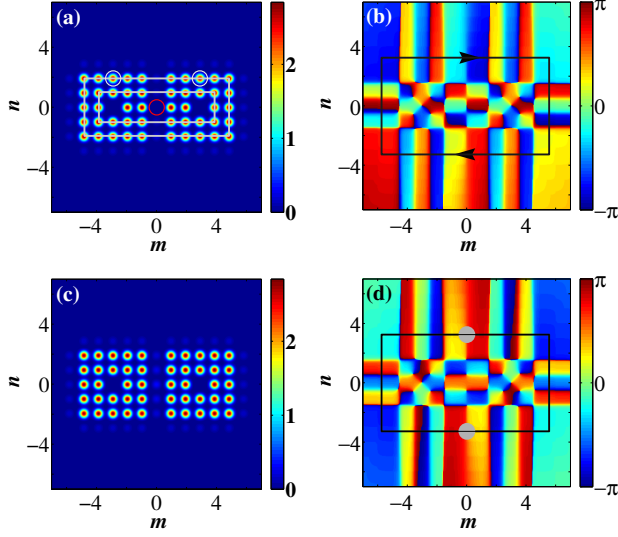


Figure 3. (Color online) Color map plots showing the amplitude (left) and phase (right) profiles for the stable solutions corresponding with the basins of attraction shown in Fig.4. For basins $\mathbf{b1}^{\leftrightarrow}$ the stable vortex soliton is similar to the profiles shown in (a) and (b). Profiles for the $\mathbf{b2}$ basin looks slightly different and are shown in (c) and (d).

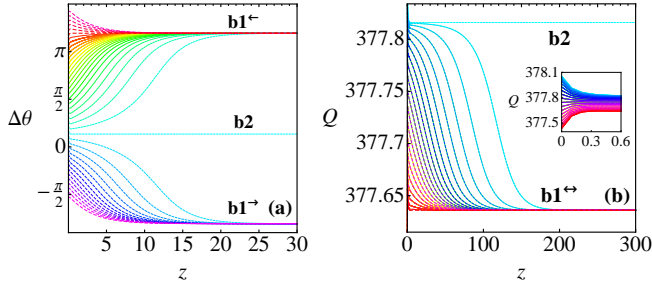


Figure 4. (Color online) (a) Dynamic evolution of the relative phase between the two sites enclosed by the white circles in the vortex solutions shown in Fig.(3). (b) Optical power evolution for the same vortex solutions. The inset in (b) shows a magnification of the initial stage of evolution.

arrows in this contour, with an accumulated charge of $S = 11$. On the other hand, if we look how the phase changes along the rectangle sketched in Fig.3(d), we see that the topological charge is not well defined on this contour. Indeed, the topological charge is truncated (see gray filled circles) meaning that this structure is not a composed vortex beam. Nevertheless, this profile can be thought as two non-interacting vortex solitons with a π radians rotation between them. As we can see from Fig.4(a), any small variation in the phase leads to this bound solution to evolve towards the basin of attraction $\mathbf{b1}^{\leftrightarrow}$. No other initial condition goes to $\mathbf{b2}$, meaning that this is not properly a basin of attraction. So, we can say that vorticity is a necessary condition, achieved during the propagation, for the stability of this kind of structures.

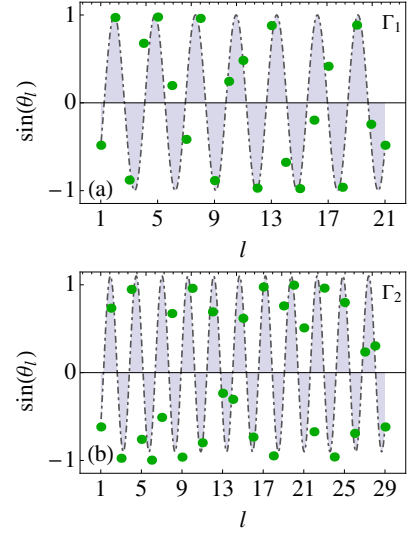


Figure 5. (Color online) $\sin(\theta_l)$ versus l for contours (a) Γ_1 and (b) Γ_2

For the sake of clarity, we plot $\sin(\theta_l)$ vs l , where l corresponds to the site on the inner (Γ_1) and outer (Γ_2) discrete contours sketched in Fig.3(a). Fig.5(a) shows a good correspondence between the data (green points) and a sinusoidal function (gray line) with seven periods ($S = 7$) along the twenty one sites of the Γ_1 contour. For the Γ_2 contour, which contains twenty nine sites, we count eleven periods ($S = 11$) as shown in Fig.5(b). Fig.5 explicitly shows the different topological charges contained simultaneously in this solution. This supports the right identification of discrete vortex solitons, which is not an easy task for discrete systems.

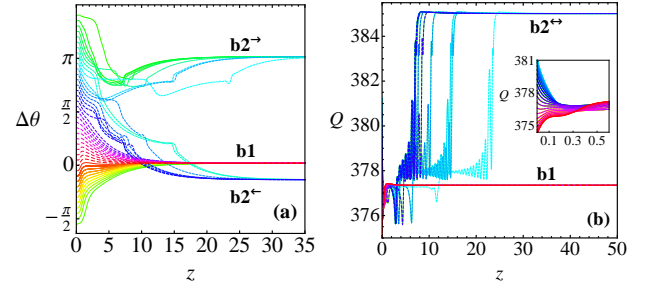


Figure 6. (Color online) (a) Dynamic evolution of the relative phase between two sites enclosed by the white circles, on the bound states showed in Fig.(7). (b) optical power evolution for the same bound state. The inset in (b) shows a magnification of the initial stage of evolution.

We consider now a second initial configuration where the two initially independent \mathbf{E} -family vortices are placed closer to each other. We find a similar evolution than before but now, there are three different stable attraction basins for the relative phase evolution [see Fig.6(a)]. Two of them, the lowest ($\mathbf{b2}^{\leftarrow}$) and the highest ($\mathbf{b1}^{\rightarrow}$), cor-

respond to the larger Q -value basin [$\mathbf{b2}^{\leftrightarrow}$ in Fig.6(b)]. The amplitude and phase profiles for these two vortices solutions are shown in Figs.7(a) and (b), and (c) and (d), respectively. We can see from the amplitude profiles that these solutions lost one of the two original central cores (both solutions are equivalent if we perform a inversion symmetry through the \hat{n} -axis). The global vorticity is lost, and we can see from Figs.7(b) and (d) how the phase circulation is truncated when we move to the region without a core. Here, we claim that this mixed bound state is composed of an **E**-family vortex soliton and a staggered bright soliton (with a π -phase shift between nearest neighbors).

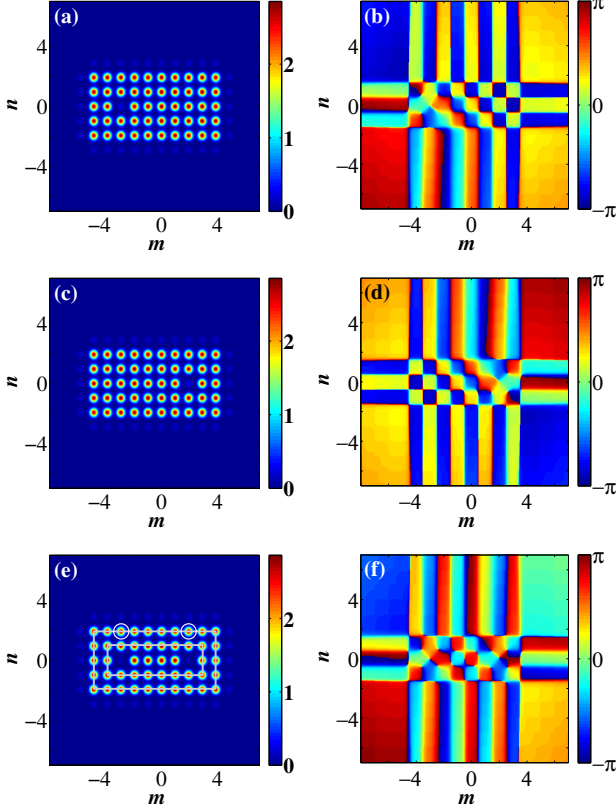


Figure 7. (Color online) Color map plots showing the amplitude (left) and phase (right) profiles for the stable solutions corresponding with the basins of attraction showed in Fig.6. For basin $\mathbf{b2}^{\leftarrow}$ the stable structure is similar to the profiles shown in (a) and (b), while (c) and (d) correspond with $\mathbf{b2}^{\rightarrow}$. For the remaining $\mathbf{b1}$ basin, the vortex soliton is similar to the profiles shown in (e) and (f).

The third basin ($\mathbf{b1}$), which corresponds to the lower Q -value basin in Fig.6(b), has the amplitude and phase profiles displayed in Figs.7(e) and (f). We clearly see that it preserves the initial two central cores keeping the same topological charge as the initial condition. Unlike the previous two basins, the global topological charge of this solution is well-defined. As for the first configuration, there are also two different topological charges for this composite vortex soliton. Again, to corroborate this, we

plot $\sin(\theta_l)$ vs l in order to show in detail the topological charge along two different contours. The first one, Γ_3 , corresponds to the inner rectangular contour sketched in Fig.7(e), while Γ_4 corresponds with the outer rectangular contour sketched in the same figure. Fig.8(a) shows how the inner charge is $S = 7$ while Fig.8(b) indicates a charge $S = 11$ for contour Γ_4 .

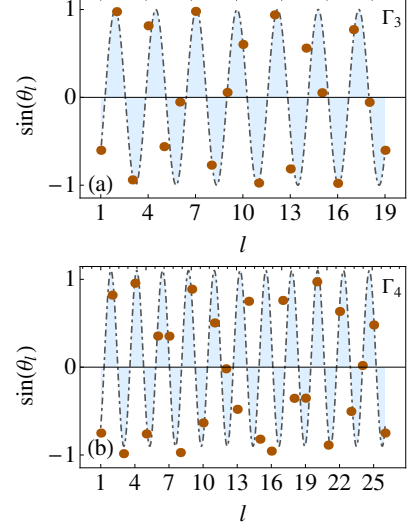


Figure 8. (Color online) $\sin(\theta_l)$ vs l (site number) diagram for the first (a) and second (b) discrete contours shown on the Fig.6(a) for the bound state vortex soliton.

We show now two more examples of composite structures built from an initial superposition of two- and four-solutions taken from the **D** and **E** families shown in Fig.1. In both cases, the values of the parameters used are: $C = 0.8$, $\delta = -0.9$, $\varepsilon = 0.9$, $\mu = -0.1$ and $\nu = 0.1$. The typical propagation distance was $z \approx 300$, enough for the power content to become constant.

Figure 9 shows three stable solutions obtained by superposing two vortex solitons belonging to the **D**-family in Fig.1. The first one is constructed by overlapping two of these vortices spaced by one site between their central cores. Figs.9(a) and (b) show the amplitude and phase profiles for this stable solution. We note that this state has only one central core, located halfway between the initial ones. On the other hand, the phase profile shows a charge $S = 5$ at the inner contour and rotated with respect to the next discrete contours.

The next configuration is constructed in the same manner as the previous one but now, the center-to-center distance between the cores has been increased to two sites. Figure 9(c) shows a dynamically stable solution with two central cores located at the same positions as the initial condition. The phase profile [see Fig.9(d)] shows a value of $S = 5$ for the topological charge, as in the previous case. A third stable composed structure is obtained by superposing again two vortex solitons with an initial center-to-center distance of three sites. The amplitude profile for the new dynamically stable solution has one

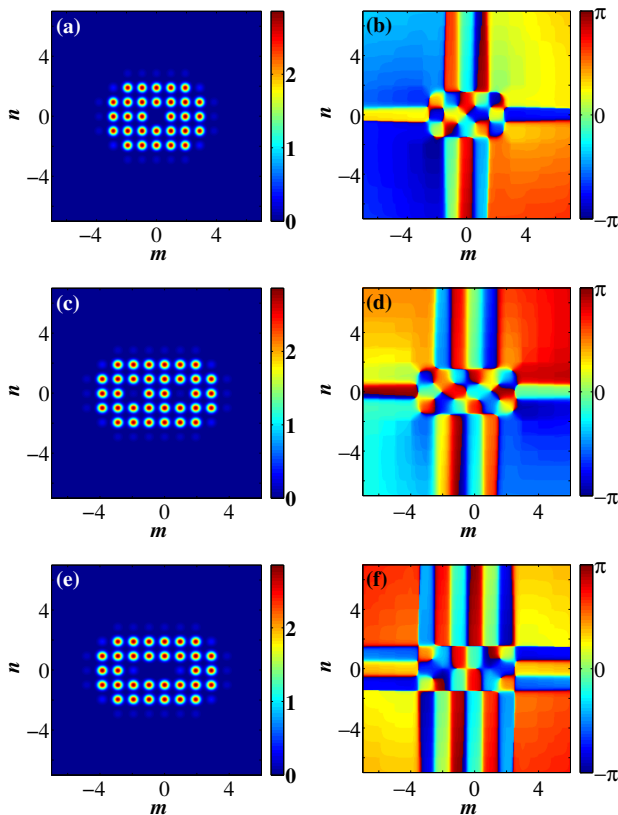


Figure 9. (Color online) Color map plots showing the amplitude (left) and phase (right) profiles for three stable vortex solutions obtained by superposing two vortex solitons belonging to the D family, at different initial distances.

horizontally elongated core, along two lattice sites, as shown in Fig.9(e), and its topological charge has two different values as shown in Fig.9(f). Indeed, the innermost discrete contour exhibits a charge $S = 6$, while the remaining contours have a charge $S = 10$.

Finally, we show another example of a composed structure that was obtained by combining four solutions belonging to the E family. We locate each E -vortex by placing their central cores forming the vertices of a 8×8 square. We use this configuration as initial condition for model (1) and find a dynamically stable stationary solution. Figs. 10(a) and (b) show the amplitude and phase profiles for this composite solution. We observe a spatial amplitude distribution similar to the initial condition, where the four initial cores preserve their initial position and vorticity. In addition, an extra phase core appears at the lattice center ($n, m = 0$), around which a $S = -1$ topological charge can be observed. If we follow a new contour that encloses all the sites with large amplitude, the topological charge measured will be $S = 15$.

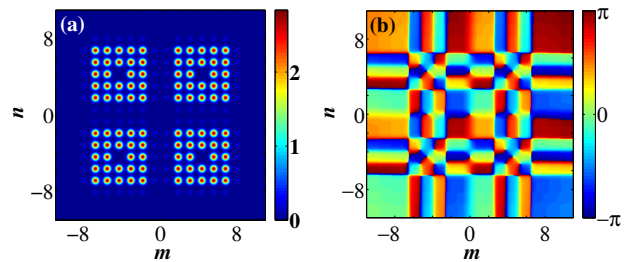


Figure 10. (Color online) Color map plots for the amplitude (a) and phase (b) profiles for a dynamically stable solution obtained by combining four solutions belonging to the E family

V. SCHRÖDINGER LIMIT

Most of the present experiments with optical beams are performed under conditions that closely meet the cubic conservative limit. So, we are interested in knowing if all these previous dissipative structures can be observed also here. In this scenario, all the dissipative parameters are suppressed, i.e., $\nu = \mu = \varepsilon = \delta = 0$, and model (3) reduces to the discrete NLSE equation

$$-\lambda\psi_{m,n} + \hat{C}\psi_{m,n} + |\psi_{m,n}|^2\psi_{m,n} = 0. \quad (7)$$

Taking as an *ansatz* for the decoupled limit for some of the solutions previously described, we have obtained the same kind of structures for the discrete NLSE. We have constructed the corresponding families and also computed their corresponding stability region. We note that all these solutions exist in the Schrödinger limit, but are stable only for high values of their optical power content.

In Fig.(11) we show five families of stationary solutions of the NLSE that correspond with some of the solutions reported in the previous sections. Namely, the blue line is the family corresponding with the solution displayed in Fig.(3a-b), the black line with the Fig.(7e-d), and the red, green and gray line with Fig.(9a-b), Fig.(9c-d) and Fig.(9e-f) respectively. The stable (unstable) solutions are represented by continuous (dashed) lines. The inset located in the upper left corner at Fig.(11) shows a magnified view of the region close to the linear band (gray zone). As usual [22], each one of these families tends to increase its power steeply after passing through the point of minimum optical power. The other inset at the lower right corner shows a zoom of the black and blue curves, which are almost indistinguishable because they have very similar spatial profiles.

VI. SUMMARY AND CONCLUSIONS

We have reported several new families of discrete vortex solitons, characterized for having two topological charges simultaneously, and coexisting for the same set of parameters. By superposing two or more of these vortices, we have been able to produce new, dynamically

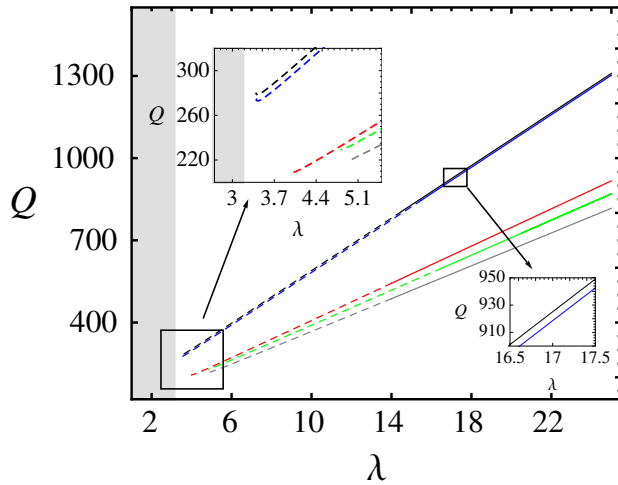


Figure 11. Q versus λ diagram displaying the families corresponding with some of dissipative solutions reported previously, but for the conservative cubic case.

stable composite vortex solitons that are also endowed with multiple vorticity charges. Additionally, we have shown that these composite structures persist in the conservative limit and they are stable for high values of their power content.

VII. ACKNOWLEDGMENTS

C.M.C. and J.M.S.C. acknowledge support from the Ministerio de Ciencia e Innovación under contracts FIS2006-03376 and FIS2009-09895. R.A.V. and M.I.M. acknowledge support from Fondecyt Grants 1110142 and 1080374, and Programa de Financiamiento Basal de Conicyt (FB0824/2008).

-
- [1] G. Molina-Terriza, J. P. Torres, and L. Torner, *Phys. Rev. Lett.* **88**, 013601 (2001).
 - [2] A. Mair, G. Weihs, and A. Zeilinger, *Nature* **412**, 313 (2001).
 - [3] A. Ashkin, J. M. Dziedzic, and T. Yamane, *Nature* **330**, 769 (1987).
 - [4] J. Scheuer and M. Orenstein, *Science* **285**, 230 (1999).
 - [5] S. D. Ganichev, E. L. Ivchenko, S. N. Danilov, J. Eroms, W. Wegscheider, D. Weiss, and W. Prettl, *Phys. Rev. Lett.* **86**, 4358 (2001).
 - [6] Y. V. Kartashov, B. A. Malomed, and L. Torner, *Rev. Mod. Phys.* **83**, 247 (2011).
 - [7] C. Sulem and P.-L. Sulem, eds., *The Nonlinear Schrödinger Equation: Self-Focusing and Wave Collapse*, vol. 139 of *Applied Mathematical Sciences* (Springer, Berlin, 1999).
 - [8] R. Conte and M. Musette, *Pure and Applied Optics: Journal of the European Optical Society Part A* **4**, 315 (1995).
 - [9] N. Akhmediev and A. Ankiewicz, eds., *Dissipative Solitons*, vol. 661 of *Lecture Notes in Physics* (Springer, Berlin, 2005).
 - [10] N. Akhmediev and A. Ankiewicz, eds., *Dissipative Solitons: From optics to biology and medicine*, vol. 751 of *Lecture Notes in Physics* (Springer, Berlin, 2008).
 - [11] I. S. Aranson and L. Kramer, *Rev. Mod. Phys.* **74**, 99 (2002).
 - [12] H. Altug, D. Englund, and J. Vuckovic, *Nature* **2**, 484 (2006).
 - [13] J. Soto-Crespo, N. Akhmediev, and A. Ankiewicz, *Physics Letters A* **314**, 126 (2003), 0375-9601.
 - [14] K. ichi Maruno, A. Ankiewicz, and N. Akhmediev, *Physics Letters A* **347**, 231 (2005), 0375-9601.
 - [15] N. K. Efremidis, D. N. Christodoulides, and K. Hizanidis, *Phys. Rev. A* **76**, 043839 (2007).
 - [16] A. S. Desyatnikov, M. R. Dennis, and A. Ferrando, *Phys. Rev. A* **83**, 063822 (2011).
 - [17] B. A. Malomed and P. G. Kevrekidis, *Phys. Rev. E* **64**, 026601 (2001).
 - [18] D. N. Neshev, T. J. Alexander, E. A. Ostrovskaya, Y. S. Kivshar, H. Martin, I. Makasyuk, and Z. Chen, *Phys. Rev. Lett.* **92**, 123903 (2004).
 - [19] E. Arévalo, *Phys. Rev. Lett.* **102**, 224102 (2009).
 - [20] J. M. Soto-Crespo, N. Akhmediev, C. Mejía-Cortés, and N. Devine, *Opt. Express* **17**, 4236 (2009).
 - [21] V. Skarka, N. B. Aleksić, H. Leblond, B. A. Malomed, and D. Mihalache, *Phys. Rev. Lett.* **105**, 213901 (2010).
 - [22] C. Mejía-Cortés, J. M. Soto-Crespo, M. I. Molina, and R. A. Vicencio, *Phys. Rev. A* **82**, 063818 (2010).
 - [23] C. Mejía-Cortés, J. M. Soto-Crespo, R. A. Vicencio, and M. I. Molina, *Phys. Rev. A* **83**, 043837 (2011).
 - [24] D. Pelinovsky, P. Kevrekidis, and D. Frantzeskakis, *Physica D: Nonlinear Phenomena* **212**, 20 (2005).
 - [25] N. N. Akhmediev, A. Ankiewicz, and J. M. Soto-Crespo, *Phys. Rev. Lett.* **79**, 4047 (1997).